NANO
LETTERS

2007
Vol. 7, No. 11
3260−3265

Ab Initio Study of Vibrational Dephasing of Electronic Excitations in Semiconducting Carbon Nanotubes

Bradley F. Habenicht,[†] Hideyuki Kamisaka,[†,‡] Koichi Yamashita,[‡] and Oleg V. Prezhdo*,[†]

Department of Chemistry, University of Washington, Seattle, Washington 98195-1700,
and Department of Chemical System Engineering, University of Tokyo,
7-3-1 Hongo, Bunkyo-ku, Tokyo 113-8656, Japan

Received May 7, 2007; Revised Manuscript Received August 1, 2007

ABSTRACT

Phonon-induced dephasing of electronic transitions in semiconducting single-wall carbon nanotubes (CNT) is investigated by ab initio molecular dynamics. Pure-dephasing is shown to be the source of the photoluminescence linewidths observed experimentally in isolated CNTs at low and room temperatures. In ideal tubes, the dephasing is found to occur by coupling to optical phonons. The dephasing proceeds notably faster in the presence of some defects due to stronger coupling to local modes, suggesting that the defects can be identified in CNTs by broadened optical bands.

Carbon nanotubes (CNT) are one of the most intriguing and robust elements of the emerging nanotechnology field. Their potential in numerous applications, ranging from quantum wires[1] to field effect transistors[2] to incorporation in photovoltaic devices[3] has led to the exertion of great effort in the scientific community to elucidate their electronic, chemical, vibrational, and optical properties.[4] Of particular interest for incorporation into nanoscale applications is the understanding of a CNTs' response to optical stimulation.[5−7]

Synthesis and purification is one of the greatest challenges faced by the community studying nanotubes. The electronic structure of CNTs is intimately linked to the twist (or chiral angle) the carbon atoms take as they build these nanoscale cylinders.[8] The extreme conditions during synthesis and large distribution of possible chiral angles and diameters make it difficult to separate and isolate single CNTs. Optical measurements on bundles or ropes of CNTs lose much of the fine spectral structure. However, in the past few years great strides have been made. Among the most important gains to the spectroscopic area was the separation of individual tubes in solution.[9] This was quickly followed by a mapping of the optical structure of individual tubes.[10] This separation of individual nanotubes from bundles has also allowed for photoluminescence studies and probing the intrinsic CNT excitations by interaction with light.[11] The synthesis of CNT samples greatly enriched in a single species is one of the most promising current advances.[12,13]

Because of improvement in the processing and production of CNTs, applications in molecular and quantum information technology are moving forward.[14] Electron−phonon interaction[15] and phonon-induced electronic dephasing[16] play key roles in many applications. For instance, the response times of logic gates,[17] optical switches,[18] and lasers[19] based on CNTs depend on the electron−phonon coupling. Energy loss that determines the conductivity of CNT wires[20,21] and field-effect transistors[22,23] occurs by charge-phonon scattering. Electron−phonon interactions provide a mechanism for the observed superconductivity of CNTs[24,25] and create distortions in tube geometric structure.[26] Quantum dephasing due to the electron−phonon coupling sets limits on coherent spin[27] and charge[28] transport through CNTs.

Vibrationally induced dephasing may be directly measured using photoluminescence (PL), photoluminescence excitation, and fluorescence spectroscopy via the absorption or emission linewidths. Several groups have reported spectral linewidths varying from 10−30 meV at room temperature[9,29−32] and even ultrathin linewidths of 0.25 meV at 50 K.[33] Investigation of the shape and temperature dependence of the PL linewidth features have shown two distinct types, which have been attributed to the ideal and unintentionally doped species,[33] suggesting that CNT defects may be identified by studying quantum dephasing.

In this letter we report the first ab initio study of the phonon-induced pure-dephasing of the electronic excitations

---

* Corresponding author. E-mail: prezhdo@u.washington.edu.
[†] University of Washington.
[‡] University of Tokyo.

10.1021/nl0710699 CCC: $37.00

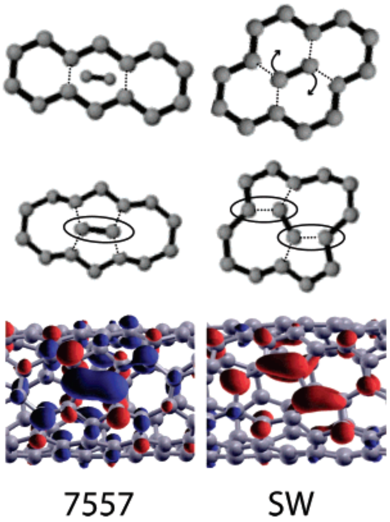

Figure 1. Defects imposed on (6,4) CNT and their relation to the ideal hexagonal lattice. The dotted lines represent bonds broken and formed to create the defects. The 7557 defect (left column) is produced by insertion of a C−C dimer across a hexagonal carbon cell. The SW defect (right column) appears due to rotation of one of the C−C bonds. The bottom panels show the transition densities corresponding to the lowest energy excitations generated in the CNT by the defects. Red and blue colors represent the positive and negative changes in the charge densities created by the excitations.

in a series of CNTs at low and ambient temperatures with and without defects. The results of the atomistic molecular dynamics (MD) simulations agree very well with the available experimental data in both temperature regimes and allow us to establish the vibrational modes that are responsible for the electronic dephasing. We show that the loss of phase information proceeds notably faster in the presence of those defects that significantly perturb the geometric structure of CNT and create local vibrational modes. Faster dephasing corresponds to larger linewidths that can be used to identify defect states.

The study focuses on the (6,4), (8,4), and (7,0) CNTs. These tubes, three of the smallest semiconducting CNTs, were chosen to achieve statistically converging results by ab initio MD. The diameters of the (7,0), (6,4), and (8,4) CNTs are 5.5, 6.8, and 8.3 Å, respectively. (7,0) is the smallest semiconducting CNT and is greatly strained due to its small diameter. The (6,4) and (8,4) tubes represent the two "$(n - m) \bmod 3 = 2$" and "$(n - m) \bmod 3 = 1$" families of the semiconducting (n, m) tubes. In addition, two common defects,[34] the 7557 and Stone−Wales (SW) defects, were introduced into the (6,4) tube with one defect per unit cell. A rotation of a C−C bond, the SW defect creates two five-membered rings and two seven-membered rings (Figure 1). The 7557 defect occurs by insertion of a C−C dimer into the middle of a benzene rings on a CNT cylinder. The 7557 defect also creates two pentagon-shaped rings and two heptagon-shaped rings, although with different orientations to one another than those imposed by the SW defect. The 7557 defect distorts the CNT geometry more strongly than the SW defect, protruding from the surface of the tube.[34]

Figure 1 also shows the excitation densities of the lowest energy excited states created by the two defects. The 7557 state is more localized than the SW state. The excitation of the 7557 defect displaces the electron density from the inserted C−C bond to the nearby carbon atoms. The SW defect has the opposite effect. The electron density shifts from a broad area of the tube onto two of the newly formed bonds. For a detailed description of these CNT defects, please see the work of Sternberg et al.[34]

The final consideration was a comparison of the dephasing of the (6,4) CNT at 300 and 50 K.

The calculations were performed with the Vienna Ab Initio Simulations Package[35] using the Perdew−Wang generalized gradient approximation[36] and Vanderbilt ultrasoft pseudopotentials.[37] The density functional theory (DFT) used here is a quasi-particle formalism that can successfully predict many electronic properties of CNTs, including optical transitions.[38,39] The electron−hole correlations, manifested in CNTs by excitonic signatures in the optical properties,[11] are implicitly included in DFT through the exchange-correlation functional. Periodic boundary conditions and a converged plane-wave basis were employed. A vacuum of 8 Å on each side of the nanotube was added to avoid nonphysical tube−tube interactions. Initial nanotube structures were obtained using Tubegen.[40] The nanotube geometry and simulation cell were then relaxed to obtain minimum energy structures. The nanotubes were then brought to 300 K (50 K) by repeated velocity rescaling. A 3.5 ps microcanonical trajectory was then generated using the Verlet integration algorithm with the ground state Hellmann−Feynman forces.

The line shape of optical absorption and emission has been extensively studied, and its theory is quite advanced.[41,42] The observed linewidth can be decomposed into an inhomogeneous term, which accounts for the distribution of optically active species and their different local environments, and a homogeneous term that is fundamental to the species of interest. Neglecting the inhomogeneous broadening in correspondence with the single-tube experiments,[9,29−33] the linewidth Γ is determined by the dephasing time, T_2, composed of the excited-state lifetime T_1 and the pure-dephasing time T_2^*:

$$\Gamma = \frac{1}{T_2} = \frac{1}{T_1} + \frac{1}{T_2^*} \qquad (1)$$

If the excited-state lifetime is much longer than the pure-dephasing time, Γ is determined by the pure-dephasing. Recent experiments[30,43] and theoretical calculations[44,45] on fluorescence of single-walled CNTs have produced excited-state lifetime expectancies on the order of nanoseconds, validating this assumption. Pure-dephasing is associated with fluctuations in the electronic energy levels due to interactions with other subsystems, such as phonons or solvent. In our present calculation, pure-dephasing occurs solely via interaction of the electronic subsystem with CNT phonons.

We begin our analysis of the dephasing times by calculating the autocorrelation function (ACF) of the CNT lowest electronic excitation energy:

$$C(t) = \langle \Delta E(t) \Delta E(0) \rangle_T \qquad (2)$$

The ACF is unnormalized and the brackets denote thermal averaging over a canonical ensemble of initial conditions. Oscillation and decay of the ACF characterize the electron−phonon interaction memory. The integral of the ACF enters one of the definitions of the pure-dephasing function (see eqs 4 and 5). Figure 2 compares the ACFs for the lowest electronic excitations of the ideal (6,4) tube at 300 and 50 K, and the (6,4) tube with the 7557 and SW defects at 300 K. The initial values of the ACF give the average fluctuation of the excitation energy due to coupling to phonons. Note that the left and right sections of Figure 2 have different time scales and that all panels have different *y*-axis scales. The ACF functions decay much more slowly in the ideal tubes than in the tubes with the defects. Comparing the ideal tubes at the ambient and low temperatures, we observe that the ACF at 300 K decays in just under a picosecond, while the ACF at 50 K has decayed little in the same amount of time. The energy fluctuation is also an order of magnitude larger at 300 K. Contrastingly, the ACF decays very rapidly within tens of a femtosecond for the tubes with the defects at room temperature. This is due to the geometric disorder and a wider range of vibrational modes available in these tubes. The 7557 defect induces a faster decay of the ACF than the SW defect, and the 7557 ACF is less symmetric with respect to the time axis. The amplitudes of the energy fluctuation form the following sequence for the (6,4) tubes at 300 K in decreasing order: ideal, SW defect, and 7557 defect. This sequence correlates with the localization of the electronic excitation and the number of carbon atoms that are able to couple to the electronic subsystem.

The CNT phonon modes that contribute to the decay of the ACF (2) and that are responsible for the pure-dephasing are analyzed in Figure 3. The Figure 3 presents the Fourier transforms (FT) of the ACFs, known as the influence spectrum.[41] The top panel presents the data for the three ideal tubes, and the bottom panels compares the ideal (6,4) tube with the tube perturbed by the defects. All FTs shown are based on the 300 K simulations. The ideal (6,4) tube at 50 K exhibits the same frequencies as the (6,4) tube at 300 K. The electronic excitation energies of the (6,4) and (8,4) CNTs fluctuate primarily due to coupling to the optical G-mode around 1600 cm^{-1}. The frequency of the mode is slightly higher in the (8,4) tube due to less geometric strain and stronger chemical bonding. Note that the resolution of the FT is 22 cm^{-1}, as determined by the length of the ab initio trajectories. The calculated frequency difference between the G-modes of the (6,4) and (8,4) tubes is only twice the numerical resolution, and the true difference is likely smaller than that. The G-mode of the (7,0) tube is significantly lower due to the substantial geometric strain.

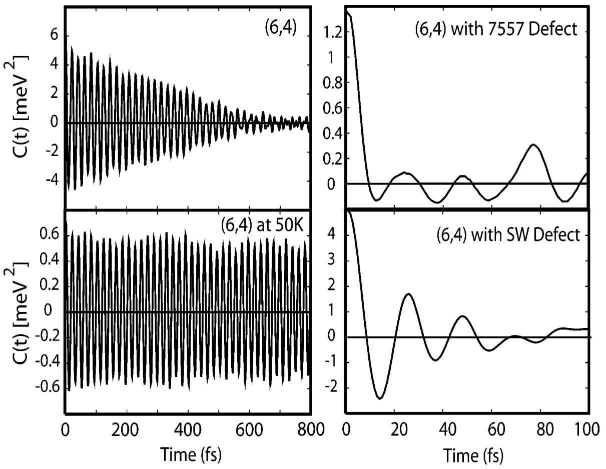

Figure 2. Energy ACFs (2) of the lowest energy excitations of the (6,4) tubes under investigation. The data for the ideal tubes show a long-lived vibrational coherence corresponding to an optical phonon. The decay is half-picosecond at room temperature and over tens of picoseconds at 50 K. In contrast, the decay occurs within 100 fs in the tubes with defects. Note that all autocorrelation functions start at different absolute magnitudes.

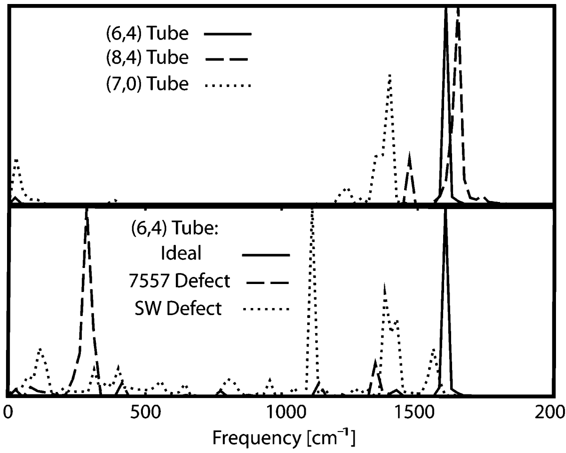

Figure 3. Fourier transforms of the ACFs (2) for the tubes studied. The tubes of ideal geometry couple primarily to the optical G-mode near 1600 cm^{-1}. The SW defect shows many disorder modes and couples to a much larger range of frequencies. The 7557 defect has a large influence on the geometry of the nanotube and most strongly interacts with a mode in the RBM frequency range.

Defects introduce a much broader range of vibrations (bottom panel of Figure 3). Stronger coupling to the radial breathing mode (RBM) and disorder modes is evident in the spectrum of the tubes with the defects. The coupling to a larger range of frequencies rationalizes the dramatically faster decay of the ACF of the tubes with defects compared to the ideal tubes (Figure 2). The SW defect couples to a very wide range of frequencies, while the 7557 defect primarily couples to a local mode in the RBM frequency range. This is due to the fundamental differences between the two defects, even though they result in similar bonding patterns (Figure 1). The SW defect is rotation of a bond, which introduces a great deal of disorder in the phonon spectrum of the whole tube. The 7557 defect, however, is an insertion of an extra C−C atom pair, which causes a bulge in the wall of the CNT[34] and creates a local vibrational mode. Because the excitation density is strongly localized on the added C−C bond, as shown in Figure 1, it is the vibration of this local structure that induces the electronic dephasing.

The vibrational normal modes generated by the 7557 and SW defects are shown in Figure 4. The 7557 defect mode is strongly localized on the inserted carbon atoms and their

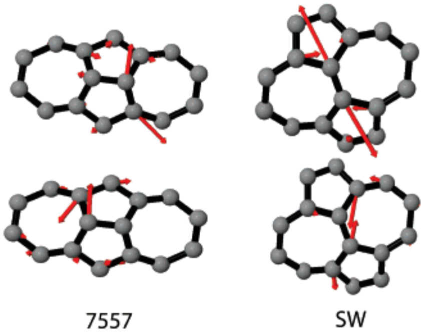

Figure 4. Defect normal modes that generate the electron−phonon coupling, which is responsible for the pure-dephasing contribution to the linewidth. The 7557 defect has a distinct frequency (Figure 3) characterized by a pair of degenerate normal modes (left column). The SW defect creates a number of frequencies (Figure 3). The top-right panel describes the high-frequency SW defect mode. The lower-right panel shows one of the many lower frequency modes, which contain small contributions from atoms outside of the defect region (not shown).

nearest neighbors. The left column of Figure 4 exhibits two degenerate 7557 modes, whose linear combinations couple to the electronic subsystem. The SW defect generates a wide range of modes with both high and low frequencies, Figure 3. The top-right panel of Figure 4 shows the high-frequency normal mode localized on the SW defect. The lower-right panel gives an example of a lower frequency mode that arises due to the defect and carries small contributions from many atoms beyond the defect part of the CNT.

The pure-dephasing function can be computed either using the ACF (2) or directly from the fluctuation of the excitation energy. In the direct method, the dephasing function is defined as[42]

$$D(t) = \exp(i\omega t)\left\langle \exp\left\{-\frac{i}{\hbar}\int_0^t \Delta E(\tau)\,\mathrm{d}\tau\right\}\right\rangle_T \qquad (3)$$

Here, ω is the thermally averaged energy gap divided by $\hbar$. The direct dephasing functions for all tubes are shown in Figure 5. The top panel depicts the results for the ideal (8,4), (6,4), and (7,0) tubes at 300 K. The lower panel presents the data for the ideal (6,4) tube at 50 and 300 K and compares the ideal tube with the defects.

One can also calculate the dephasing function using a cumulant expansion.[42] In this case, the ACF (2) is doubly integrated

$$g(t) = \int_0^t d\tau_1 \int_0^{\tau_1} C(\tau_2)\,\mathrm{d}\tau_2 \qquad (4)$$

The function $g(t)$ is then exponentiated to define the approximate dephasing function

$$D(t) = e^{-g(t)} \qquad (5)$$

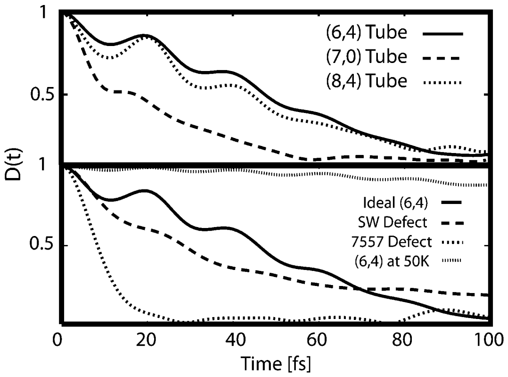

Figure 5. CNT dephasing functions calculated using eq 3. The dephasing timescales reported in Table 1 have been obtained by fitting these functions to eq 6. The upper panel compares the ideal tubes at room temperature. (6,4) and (8,4) dephase on a similar time scale, while (7,0) shows a substantially faster dephasing due to larger fluctuation of the excitation energy. The lower panel compares modifications of the (6,4) tube. The dephasing is much slower at 50 than at 300 K. The SW defect slightly speeds up the dephasing, while the 7557 defect strongly decreases the decay time scale.

Table 1. Pure-Dephasing Times T_2^* and Corresponding Homogeneous Linewidths Γ (Equation 1) Obtained by Fitting the Direct Dephasing Functions (3) Shown in Figure 5 to Equation 6[a]

tube	T_2^*(fs)	A	ω (fs^{-1})	Γ (meV)
(8,4)	51.2	0.061	0.30	12.8
(7,0)	23.2	0.10	0.29	28.2
(6,4)	59.6	0.086	0.32	11.0
7557	10.2	0		64.6
SW	48.0	0.062	0.25	13.7
50 K	955	0.0056	0.30	0.69

[a] (8,4), (7,0), and (6,4) refer to the ideal tubes at room temperature; 7557 and SW are defects in the (6,4) tube shown in Figure 1; and 50 K indicates the (6,4) tube at the low temperature.

Table 2. Pure-Dephasing Times T_2^* and Corresponding Homogeneous Linewidths Γ (Equation 1) Obtained by Fitting the Cumulant Dephasing Function (5) to Equation 6[a]

tube	T_2^*	A	ω (fs^{-1})	Γ (meV)
(8,4)	52.4	0.062	0.30	12.5
(7,0)	9.12	0		72
(6,4)	54.3	0.080	0.30	12.1
7557	10.1	0		65.2
SW	42.1	0.027	0.24	15.6
50 K	750	0.0045	0.30	0.87

[a] See footnote to Table 1.

The cumulant approximation converges much faster than the direct calculation, which is an important factor for our relatively short ab initio simulation. Comparison between the direct and cumulant data allowed us to test the convergence of our results. The approximate dephasing function agrees with the direct function (3), if the higher order cumulants beyond the second-order ACF are insignificant. The validity of the second-order approximation can be evaluated based on the fits reported in Tables 1 and 2. The approximation works in all tubes considered here except for the (7,0) tube, which exhibits long memory effects in the electron−phonon interaction. The vibrational motion of the (7,0) tube is quite anharmonic due to its small diameter and larger geometric strain. The anharmonic motion manifests itself in the asymmetric form of the tube's ACF (not shown): a particle in a skewed parabolic potential spends more time on the less steep side, creating an asymmetric ACF. The cumulant function (5) agrees well with the direct function (3) for the first 10 fs. At the later times, the cumulant function smoothly continues the rapid decay, while the direct function changes its angle and decays more slowly, similarly to the dephasing functions for the other ideal tubes.

Both direct and cumulant dephasing functions were fit by the following equation

$$f(t) = \exp\left(-\frac{t}{\tau}\right)\frac{1 + A\cos(\omega t)}{1 + A} \qquad (6)$$

The fitting parameters are shown in Tables 1 and 2, respectively. The time τ is the pure-dephasing time. The frequency ω represents the oscillation of the dephasing function, and the constant A is related to the amplitude of the oscillation. For the ideal tubes and the (6,4) tube with the SW defect, $\omega \approx 0.30$ fs^{-1} corresponds to the optical G-mode. The oscillation of the dephasing functions for the 7557 defect is rather weak.

The dephasing times of (6,4) and (8,4) tubes in the ideal geometry are between 50 and 60 fs, which correspond to linewidths of 11−13 meV (eq 1). These linewidths are within the range of 10−15meV reported by Lefebvre et al.[31] and are slightly more narrow than those reported by O'Connell et al.[9] The broader peaks seen in the latter work can be attributed to solvent or surfactant interactions with the nanotubes. The former reference investigated nanotubes grown across silicon pillars in the absence of such interactions. Because the simulations excluded solvent, our results should be compared directly with ref 31, indicating very good agreement with the experiment. The ideal (7,0) tube has a dephasing time of approximately half that of the other pristine geometry tubes (Table 1). The faster dephasing is attributed to the larger fluctuation of the excitation energy and coupling to a broader range of phonon modes (Figure 3). The (7,0) linewidth still is within the experimental range.

The two defects have remarkably different effects on the dephasing time. The 7557 defect accelerates the dephasing by a factor of 6. This is due to strong electronic coupling to a local vibrational mode created by the defect. The coupling is notably anharmonic, as indicated by the asymmetric form of the ACF (Figure 2). The SW defect accelerates the dephasing only slightly. Even though the electronic excitation localized on the SW defect couples to a wider range of phonons, the coupling is harmonic and relatively weak due to the delocalized nature of the SW defect state. On the basis of the magnitude of the fluctuation of the excitation energy alone, which is larger for the SW defect than for the 7557 defect, and comparing the initial values of the ACFs in Figure 2, one might have expected faster dephasing in the SW case. This is not true, however, because the ACF of the SW state is quite symmetric, generating a significant amount of cancelation in the integral (4). The dephasing time of the (6,4) tube at 50 K is decreased by over an order of magnitude from room temperature. Our dephasing time and the corresponding linewidth is in good agreement with the reported ultrathin linewidths at 50 K.[33]

It was conjectured recently[46] that the 70 fs dephasing in CNTs may occur due to a hopping of excitons along the nanotube axis between localized potential energy minima and that suppression of the hopping at cryogenic temperatures accounts for the markedly narrower linewidths. This mechanism suggests that the observed linewidth Γ arises from the exciton lifetime T_1 between the hops (eq 1). Our calculations indicate that the pure-dephasing contribution T_2^* due to electron−phonon interaction is sufficient to explain the optical linewidth and its temperature dependence. In the presence of both a 50−60 fs vibrational dephasing and a 70 fs hopping, the linewidths would have to be nearly twice as broad, suggesting that exciton hopping is somewhat slower. This conclusion does not contradict the experimental results of ref 46, which deduced the 70 fs hopping time using order of magnitude arguments. If the hopping time is longer only by a factor 2 or 3, its contribution to the linewidth becomes much smaller than that of the pure-dephasing process.

The calculations reported here were performed for the CNT lowest excited states. While the defect states are well separated from the higher energy excitations, the picture is more complex in the ideal tubes. Depending on the tube, several low-lying excitonic bands may be thermally accessible at room temperature and can contribute to the emission process, possibly increasing the experimentally observed linewidths. This effect requires further investigation, involving nonadiabatic dynamics[47,48] that determines the occupations of multiple states.

In summary, we have calculated the dephasing times of the (6,4), (8,4), and (7,0) CNTs and investigated the role of two common defects and temperature on dephasing in the (6,4) CNT. To our knowledge, this is the first time-domain ab initio study of pure-dephasing in CNTs. The results are in excellent agreement with the experimental data measured for isolated CNTs at both low and room temperatures. The calculations suggest that CNT interaction with solvent and/or surfactants should speed up dephasing and broaden electronic transition lines by about a factor of 2. The simulation predicts that CNT defects that strongly perturbed the nanotube structure, such as the 7557 defect studied here, create electronic excitations with significantly broader transition lines. This fact is attributed to stronger electron−phonon interaction involving localized electronic states. The phonon-induced dephasing of the electronic transitions in the ideal tubes occurs by coupling to the high-frequency optical phonons. The dephasing of the defect states proceeds via local disorder and RBM modes. The theoretically predicted broader optical bands can be used to identify defect states in CNTs.

Acknowledgment. B.F.H. is supported by the Center for Nanotechnology at the University of Washington with funding from an IGERT Fellowship Award NSF #DGE-0504573. H.K. expresses his gratitude for JSPS research Fellowships for Young Scientists. K.Y. is supported by a grant-in-aid for the 21st Century COE Program "Frontiers in Fundamental Chemistry" and Scientific Research (KAKENHI) in the Priority Area "Molecular Theory for Real Systems" from the Ministry of Education, Culture, Sports, Science, and Technology of Japan. O.V.P. acknowledges financial support of ACS-PRF Grant 46772-AC6, DOE Grant DE-FG02-05ER15755, and JSPS Fellowship for Foreign Scholars and is grateful to Professor Yoshitaka Tanimura at the Kyoto University for hospitality during manuscript preparation.

References

(1) Guo, X. F.; Small, J. P.; Klare, J. E.; Wang, Y.; Purewal, M. S.; Tam, I. W.; Hong, B. H.; Caldwell, R.; Huang, L.; O'Brien, S.; Yan, J.; Breslow, R.; Wind, S. J.; Hone, J.; Kim, P.; Nuckolls, C. *Science* **2006**, *311*, 356.
(2) Javey, A.; Guo, J.; Wang, Q.; Lundstrom, M.; Dai, H. *Nature* **2003**, *424*, 654.
(3) Kongkanand, A.; Dominguez, R. M.; Kamat, P. V. *Nano Lett.* **2007**, *7*, 676.
(4) Grobert, N. *Mater. Today* **2006**, *10*, 28.
(5) Sfeir, M. Y.; Beetz, T.; Wang, F.; Huang, L. M.; Huang, X. M. H.; Huang, M. Y.; Hone, J.; O'Brien, S.; Misewich, J. A.; Heinz, T. F.; Wu, L. J.; Zhu, Y. M.; Brus, L. E. *Science* **2006**, *312*, 554.
(6) Hertel, T.; Hagen, A.; Talalaev, V.; Arnold, K.; Hennrich, F.; Kappes, M.; Rosenthal, S.; McBride, J.; Ulbricht, H.; Flahaut, E. *Nano Lett.* **2005**, *5*, 511.
(7) Hartschuh, A.; Pedrosa, H. N.; Peterson, J.; Huang, L.; Anger, P.; Qian, H.; Meixner, A. J.; Steiner, M.; Novotny, L.; Krauss, T. D. *ChemPhysChem* **2005**, *6*, 577.
(8) Saito, R.; Dresselhaus, G.; Dresselhaus, M. S. *Physical Properties of Carbon Nanotubes*; Imperial College Press: London, 1998.
(9) O'Connell, M. J.; Bachilo, S. M.; Huffman, C. B.; Moore, V. C.; Strano, M. S.; Haroz, E. H.; Rialon, K. L.; Boul, P. J.; Noon, W. H.; Kittrell, C.; Ma, J. P.; Hauge, R. H.; Weisman, R. B.; Smalley, R. E. *Science* **2002**, *297*, 787.
(10) Bachilo, S. M.; Strano, M. S.; Kittrell, C.; Hauge, R. H.; Smalley, R. E.; Weisman, R. B. *Science* **2002**, *298*, 2361.
(11) Wang, F.; Dukovic, G.; Brus, L. E.; Heinz, T. F. *Science* **2005**, *308*, 838.
(12) Zheng, M.; Jagota, A.; Strano, M. S.; Santos, A. P.; Barone, P.; Chou, S. G.; Diner, B. A.; Dresselhaus, M. S.; Mclean, R. S.; Onoa, G. B.; Samsonidze, G. G.; Semke, E. D.; Usrey, M.; Walls, D. J. *Science* **2003**, *302*, 1545.
(13) Hertel, T.; Zhu, Z.; Crochet, J.; McPheeters, C.; Ulbrecht, H.; Resasco, D. *Phys. Status Solidi B* **2006**, *243*, 3186.
(14) Avouris, P.; Chen, J. *Mater. Today* **2006**, *9*, 46.
(15) Shreve, A. P.; Haroz, E. H.; Bachilo, S. M.; Weisman, R. B.; Tretiak, S.; Kilina, S.; Doorn, S. K. *Phys. Rev. Lett.* **2007**, *98*, 037405.
(16) Roche, S.; Jiang, J.; Triozon, F.; Saito, R. *Phys. Rev. Lett.* **2005**, *95*, 076803.
(17) Mason, N.; Biercuk, M. J.; Marcus, C. M. *Science* **2004**, *303*, 655.
(18) Chen, Y.-C.; Raravikar, N. R.; Schadler, L. S.; Ajayan, P. M.; Zhao, Y.-P.; Lu, T.-M.; Wang, G.-C.; Zhang, X.-C. *Appl. Phys. Lett.* **2002**, *81*, 075.
(19) Set, S. Y.; Yaguchi, H.; Tanaka, Y.; Jablonski, M. *IEEE J. Quantrum Electron.* **2004**, *10*, 137.
(20) Terabe, Y.; Hasegawa, T.; Nakayama, T.; Aono, M. *Nature* **2005**, *433*, 47.
(21) Tans, S. J.; Devoret, M. H.; Dai, H. J.; Thess, A.; Smalley, R. E.; Geerligs, L. J.; Dekker, C. *Nature* **1997**, *386*, 474.
(22) Misewich, J. A.; Martel, R.; Avouris, P.; Tsang, J. C.; Heinze, S.; Tersoff, J. *Science* **2003**, *300*, 783.
(23) Weitz, R. T.; Zschieschang, U.; Effenberger, F.; Klauk, H.; Burghard, M.; Kern, K. *Nano Lett.* **2007**, *7*, 22.
(24) Tang, Z. K.; Zhang, L. Y.; Wang, N.; Zhang, X. X.; Wen, G. H.; Li, G. D.; Wang, J. N.; Chan, C. T.; Sheng, P. *Science* **2001**, *292*, 2462.
(25) Bohnen, K. P.; Heid, R.; Liu, H. J.; Chan, C. T. *Phys. Rev. Lett.* **2004**, *93*, 245501.
(26) Tretiak, S.; Kilina, S.; Piratinski, A.; Saxena, A.; Martin, R. L.; Bishop, A. R. *Nano Lett.* **2007**, *7*, 86.
(27) Hueso, L. E.; Pruneda, J. M.; Ferrari, V.; Burnell, G.; Valdes-Herrera, J. P.; Simons, B. D.; Littlewood, P. B.; Artacho, E.; Fert, A.; Mathur, N. D. *Nature* **2007**, *445*, 410.
(28) Jarillo-Herrero, P.; van Dam, J. A.; Kouwenhoven, L. P. *Nature* **2006**, *439*, 953.
(29) Hartschuh, A.; Pedrosa, H. N.; Novotny, L.; Krauss, T. D. *Science* **2003**, *301*, 1354.
(30) Jones, M.; Engtrakul, C.; Metzger, W. K.; Ellingson, R. J.; Nozik, A. J.; Heben, M. J.; Rumbles, G. *Phys. Rev. B* **2005**, *71*, 115426.
(31) Lefebvre, J.; Finnie, P.; Homma, Y. *Phys. Rev. B* **2004**, *70*, 045419.
(32) Inoue, T.; Matsuda, K.; Murakami, Y.; Maruyama, S.; Kanemitsu, Y. *Phys. Rev. B* **2006**, *73*, 233401.
(33) Htoon, H.; Connell, M. J. O.; Cox, P.; Doorn, S. K.; Klimov, V. I. *Phys. Rev. Lett.* **2004**, *93*, 027401.
(34) Sternberg, M.; Curtiss, L. A.; Gruen, D. M.; Kedziora, G.; Horner, D. A.; Redfern, P. C.; Zapol, P. *Phys. Rev. Lett.* **2006**, *96*, 075506.
(35) Kresse, G.; Furthmüller, J. *Comput. Mater. Sci.* **1996**, *6*, 15−50.
(36) Perdew, J. P. In *Electronic Structure of Solids*; Ziesche, P., Eschrig, H., Eds.; Akademie Verlag: Berlin, 1991.
(37) Vanderbilt, D. *Phys. Rev. B* **1990**, *41*, 7892.
(38) Barone, V.; Peralta, J. E.; Wert, M.; Heyd, J.; Scuseria, G. E. *Nano Lett.* **2005**, *5*, 1621.
(39) Capaz, R. B.; Spataru, C. D.; Tangney, P.; Cohen, M. L.; Louie, S. G. *Phys. Rev. Lett.* **2005**, *94*, 036801.
(40) Frey, J. T.; Doren, D. J. *TubeGen 3.3*; University of Delaware: Newark, DE, 2005.
(41) Skinner, J. L. *Ann. Rev. Phys. Chem.* **1988**, *39*, 463.
(42) Mukamel, S. *Principles of Nonlinear Optical Spectroscopy*; Oxford University Press: New York, 1995.
(43) Sheng, C. X.; Vardeny, Z. V.; Dalton, A. B.; Baughman, R. H. *Synth. Met.* **2005**, *155*, 254.
(44) Spataru, C. D.; Ismail-Beigi, S.; Capaz, R. B.; Louie, S. G. *Phys. Rev. Lett.* **2005**, *95*, 247402.
(45) Perebeinos, V.; Tersoff, J.; Avouris, P. *Nano Lett.* **2005**, *5*, 2495.
(46) Cognet, L.; Tsyboulski, D. A.; Rocha, J.-D. R.; Doyle, C. D.; Tour, J. M.; Weisman, R. B. *Science* **2007**, *316*, 1465.
(47) Craig, C. F.; Duncan, W. R.; Prezhdo, O. V. *Phys. Rev. Lett.* **2005**, *95*, 163001.
(48) Habenicht, B. F.; Craig, C. F.; Prezhdo, O. V. *Phys. Rev. Lett.* **2006**, *96*, 187401.

NL0710699